journal homepage: www.intl.elsevierhealth.com/journals/cmpb

Identification of temporal variations in mental workload using locally-linear-embedding-based EEG feature reduction and support-vector-machine-based clustering and classification techniques

*Zhong Yin, Jianhua Zhang**

Department of Automation, East China University of Science and Technology, Shanghai 200237, PR China

ARTICLE INFO

Article history:
Received 23 December 2013
Received in revised form
17 April 2014
Accepted 18 April 2014

Keywords:
Mental workload
Locally linear embedding
Support vector data description
Support vector clustering
Operator functional state

ABSTRACT

Identifying the abnormal changes of mental workload (MWL) over time is quite crucial for preventing the accidents due to cognitive overload and inattention of human operators in safety-critical human–machine systems. It is known that various neuroimaging technologies can be used to identify the MWL variations. In order to classify MWL into a few discrete levels using representative MWL indicators and small-sized training samples, a novel EEG-based approach by combining locally linear embedding (LLE), support vector clustering (SVC) and support vector data description (SVDD) techniques is proposed and evaluated by using the experimentally measured data. The MWL indicators from different cortical regions are first elicited by using the LLE technique. Then, the SVC approach is used to find the clusters of these MWL indicators and thereby to detect MWL variations. It is shown that the clusters can be interpreted as the binary class MWL. Furthermore, a trained binary SVDD classifier is shown to be capable of detecting slight variations of those indicators. By combining the two schemes, a SVC–SVDD framework is proposed, where the clear-cut (smaller) cluster is detected by SVC first and then a subsequent SVDD model is utilized to divide the overlapped (larger) cluster into two classes. Finally, three-class MWL levels (low, normal and high) can be identified automatically. The experimental data analysis results are compared with those of several existing methods. It has been demonstrated that the proposed framework can lead to acceptable computational accuracy and has the advantages of both unsupervised and supervised training strategies.

1. Introduction

With the development of sophisticated automatic control/automation techniques, human operators become the supervisors and the decision makers in human–machine systems [1–4]. However, the abnormal psychophysiological states

* *Corresponding author*. Tel.: +86 21 6425 3808.
E-mail address: zhangjh@ecust.edu.cn (J. Zhang).
http://dx.doi.org/10.1016/j.cmpb.2014.04.011

of the operator may lead to the operator performance degradation [1]. On one hand, in order to cope with the large-scale and/or time-varying information flows, operators may ignore critical clues due to the limited cognitive capacity, which adversely impacts the regular functioning of the system [5]. On the other hand, engaged with the human–machine system with high level of automation for a long duration, operators may become inattentive [3] and it could prevent them from manually coping with unforeseen emergent events in time. It is thus quite necessary to address how to maintain the optimal operator functional state (OFS) in the context of human–machine systems, where the risk of the accident is closely related to humanistic component/agent, e.g., in the fields of public transportations (driving, railway and shipping) [6–9], chemical and nuclear industry [10,11] and aeronautics and aerospace [2].

Mental workload (MWL), which fluctuates in response to the transient cognitive demand, is considered to be a crucial factor of OFS. Some researchers even use these two concepts/terms interchangeably [12]. According to the existing studies [13–16], a reasonable definition of MWL can be summarized as "the portion of the operator information processing capacity or resources that is required to meet system demands and the mental effort that the operator devotes to control or supervision". For the purpose of adapting operators to be attentive, concentrated, engaged to the primary task requirements and of avoiding MWL overload, adaptive automation strategy was proposed to allocate proper type and amount of tasks between the operator and the computer dynamically in human–machine systems [1,17–20].

The neuroimaging technologies, such as electroencephalogram (EEG) and functional magnetic resonance imaging, have been used widely and effectively to examine human brain functions related to MWL variations. In particular, EEG has the advantages of high temporal resolution and readiness of implementation. It was successfully applied in many fields combined with pattern classification techniques, such as brain computer interface [21], depression diagnoses [22], and sleep-wake classification [23]. Regarding the MWL level detection/classification issue, EEG has been extensively utilized together with other psychophysiological measurements, e.g., electrocardiogram (ECG), electrodermal measurement, and electrooculography signals [24–26]. The early work has verified that the level of MWL under different levels of task complexity and/or difficulty could be categorized into a few different classes based on temporal change of the EEG power spectral density (PSD) or the time–frequency features of the EEG time-series data [27]. These studies showed that the suppression of the parietal and occipital α (8–13 Hz) power as well as the enhancement of the frontal θ (4–7 Hz) power of EEG would occur with increased task difficulty. Moreover, when operators perform long-duration and low-cognitive-demand tasks, the inattentive state caused by monotonous task operations can be also detected by making use of measured EEG data. This issue is termed as alertness detection [6–9,28–30], where the significant change of EEG–PSD features is often used to determine the level of alertness and/or drowsiness of the operator.

On the other hand, EEG can be combined with other different psychophysiological measures to overcome the insensitivity of the single psychophysiological marker of particular individual operators [31–33], for example the EEG, ECG and ocular features were jointly utilized. In recent years, the multimodal approach also received much attention, where EEG was integrated with other neuroimaging techniques [34–36]. For instance, the combination of steady-state visual evoked potentials with EEG has been explored for establishing the reliable human–machine interaction [34]. The gaze information was embedded in the EEG-based brain–computer system [35]. In particular, the functional near infrared spectroscopy measurement for recognizing the MWL variation was also examined [36]. Using the mixed information from the multimodal approach can be beneficial for comprehensively exploring the salient features of human brain functions.

To interpret the MWL changes using the measured psychophysiological data, some statistical methods and linear classification techniques were developed, e.g., the hybrid approach by combining principle component analysis (PCA) and stepwise discriminant analysis [37]. The nonlinear classifiers, particularly artificial neural networks and support vector machines (SVM), were shown to achieve superior pattern classification performance [38–40]. More recent work was focused on extracting the most representative features to reveal the relationship between task difficulty/performance and the neurophysiological responses under virtual reality environment [7,8,41,42], where the independent component analysis technique has been widely applied for EEG data preprocessing and analysis. In addition, to achieve high classification accuracy of nonlinear classification or modeling techniques, the improved optimization methods [43] and the hybrid learning approaches [33] were also examined.

In this paper, a novel MWL detection framework based on a combination of unsupervised and supervised learning strategies are proposed to cope with several crucial issues that received less attention in the literature: (1), as multi-channel EEG recording is applied in our data acquisition experiments, the dimensionality of the candidate EEG feature vectors can be very high. Therefore, the performance of various data-driven methods may be limited due to the curse of the dimensionality, i.e., the available data in high-dimensional space is sparse and the amount of data required for eliciting the reliable results would grow exponentially with the dimensionality [44,45]. Moreover, if the number of training samples is even smaller than the number of features, the peaking phenomenon occurs and the accuracy of prediction/classification methods would be also degraded [46]. To this end, a viable solution is to automatically derive MWL features by using certain feature reduction techniques while the change of MWL can be interpreted/visualized by using a few EEG markers; (2) the intrinsic clusters of EEG features related to MWL variations are rarely explored and it could be beneficial to understand the transition of the operator's brain process involved in complex human–machine system; (3) considering the supervised learning based classification methods, the training targets of each psychophysiological sample must be known. Here, the continuously measured task performance data [47] as well as the type of control conditions is used to determine the target class labels.

To address the above three issues, a EEG-data-based MWL detection framework using integratively locally linear embedding (LLE) [48], support vector clustering (SVC) [49] and support

vector data description (SVDD) [50] is proposed and validated. In this work, LLE technique is utilized to find the low-dimensional manifold in the high-dimensional EEG feature space in order to extract the representative EEG markers from different cortical regions. This implementation is motivated by that the consistent brain process reflected by EEG–PSD time courses could form a manifold with the limited dimensionality which can be used to represent the low-dimensional MWL indicators. Moreover, EEG data is typically nonlinear and the classical linear dimension reduction method may not be adequate. It is also worth noting that LLE has been successfully used in many real world applications, e.g., feature fusion [51], image classification [52], and face recognition [53], where the representative features with the relatively low dimensionality can be elicited. Then, the SVC approach, which is used to find the data clusters in EEG data space with no need to know the number of clusters, is adopted to detect the drastic change of the EEG features. In this way, a SVC–SVDD hybrid framework is established, where the crisp cluster is first found by SVC and a subsequent SVDD model is utilized to discriminate/distinguish the somewhat blurred and overlapped cluster into two classes. The hybrid framework is shown to yield acceptable accuracy of three-class (low, normal and high) MWL temporal data classification.

This paper is organized as follows. The next section describes the principle of the experimental paradigm, EEG data preprocessing scheme and MWL detection framework. The corresponding results are shown in Section 3. In Section 4, the detailed discussions are given. Section 5 includes conclusion and future works.

2. Materials and methods

2.1. Experimental paradigm

2.1.1. Experimental environment

In the experiment, a simulated safety-critical human–machine system with the complex tasks is considered. The aim of the study is to evaluate the MWL level of the human operator on earth when coping with tasks for remotely monitoring/repairing the air quality manager systems of the spacecraft in the low earth orbit. It was provided by automation-enhanced cabin air management system (ACAMS). The original idea of ACAMS came from [2,20,54,55] and it was redeveloped by FGAIO of Technical University of Berlin. ACAMS was designed as a life support system of a micro-world with a representative process control environment. A group of control tasks require the operator to interact with the dynamic information that reflects the system status and also highly demand the operator's cognitive resources. The main task of ACAMS for the operator is to monitor the current states of the system and collaborate with the automatic controllers to maintain the quality of the breathable air in the closed cabin. Hence, the operator's performance breakdown would lead to the serious human–machine system failure and harm the safety of the human in the spacecraft. To this end, evaluating operator's MWL is crucial for preventing the high-risk operational states since the high level of MWL indicates the operator suffers the tasks that are too difficult to automate.

The dynamic visual display of ACAMS consists of four subsystems, i.e., oxygen concentration (O_2), pressure (P), carbon dioxide concentration (CO_2) and temperature (T), while each subsystem with automatic and manual control mode is highly dependent with others. Only the system control task is considered in this study, i.e., subjects were instructed to manually compensate for the drift of several subsystems and try to maintain them within the target ranges when corresponding automatic controllers were defined to be the failure. In this case, there were preprogrammed technical failures/faults of subsystems and the corresponding variables related to the air quality of the cabin cannot be automatically controlled. In order to maintain the safe functioning of the human–machine system as a whole, those subsystems have to be switched from automatic mode to manual mode, which allows human operator take over some control tasks requiring manual control due to the unavailability or failure of automatic control functionality. The operator must continue the manual control operations until the failures were detected and fixed. On one hand, the number of manually controlled subsystems (NOS) was adopted to indicate the task difficulty [47], i.e., the larger NOS represents more difficult task. Moreover, standard (SL) and high (HL) actuator sensitivity levels were defined for each subsystem, i.e., the task under the HL condition is much more difficult. Hence, there are two factors that can influence the complexity of subjects' tasks, i.e., NOS and the actuator sensitivity. On one hand, larger NOS indicates the subject has to accomplish more tasks at one time. Moreover, under HL condition, the corresponding subsystem can be compensated to the target ranges representing the safety system state very quickly. However, it demands more subjects' attention and mental resource with the dynamic display of ACAMS since the subsystems can easily run out of the target range. The reason for using both two factors is to provide enough task load difficulty to simulate the possible performance breakdown or dysfunctional situation of the human–machine system.

2.1.2. Subjects

Six volunteers participated in the experiment and had given informed consent. All subjects with the engineering background are male, healthy, right-handed and well trained for tasks. None of subjects had a history of neurological or psychiatric disorders and all of them are the postgraduates of East China University of Science and Technology, Shanghai, China. The psychophysiological data collected on five of them (subjects A–E, 22–24 years, mean age 23) were adopted in this work. The data set of one subject has been removed from the study because one part of the data has been mistakenly rewritten by another subject's data. In this case the dataset was contaminated and not correct for the subsequent analysis.

2.1.3. Experimental procedure

Each subject operated ACAMS for two trials which were performed at the same time on different days. These ten trials (5 subjects × 2 trials) are denoted as A1, A2, B1, B2,..., E1, E2, respectively. Each trial contains ten phases and lasts 50 min (i.e., each phase lasts 5 min, see Fig. 1).

Table 1 – Detailed control conditions across 10 phases.

Phase	Control mode	Operator's tasks	Actuator sensitivity
1	Auto	–	–
2	Manual/auto	O_2 and P	SL
3	Manual/auto	O_2 and P	HL
4	Auto	–	–
5	Manual/auto	O_2, P and CO_2	SL
6	Manual/auto	O_2, P and CO_2	HL
7	Auto	–	–
8	Manual	O_2, P, CO_2 and T	SL
9	Manual	O_2, P, CO_2 and T	HL
10	Auto	–	–

The control conditions across 10 phases for one trial are defined as follows. In phase 1, 4, 7 and 10 of baseline conditions, all subsystems were automatically controlled. During the phase 2 and 3, two subsystems were defined as the failure and the subject was required to manually control them under the SL and HL actuator sensitivity, respectively. Similarly, three and four subsystems were defined as the failure for the phase 5–6 and 8–9, respectively, and the subjects need to accomplish the same tasks under SL (for phase 5 and 8) and HL conditions (for phase 6 and 9). The details are listed in Table 1. It is noted that during the baseline conditions the subjects also have to monitor the trajectories of all subsystem to maintain the situation awareness of the task environment despite the manual process-control operations are not required. In this case, the subjects with opened eyes were required to concentrate themselves on the dynamic display of ACAMS because the subjects may become unfamiliar with the task operations if they were fully rested for a certain time period. Moreover, compared to our previous study [47], the length of each control condition was reduced from 15 min to 5 min and the more difficult tasks are involved with HL condition. The shorter duration of the conditions impose instantaneous demand of the cognitive resource of the operator, which is more related to MWL variations. In this case, the factor of fatigue accumulation is not a main factor that influences EEG data. On the other hand, more difficult tasks can help us examine the limit of the cognitive capacity of the operator. As a result, more reliable definition of discrete MWL levels can be made.

2.2. *Data acquisition and pre-processing*

When subjects operated with ACAMS, the psychophysiological data (EEG, ECG and ocular signal) were measured via EEG acquisition equipment (Nihon Kohden® EEG system). In this study, only EEG signals are used as clues to identify MWL variations, which were recorded by using fifteen channels on the scalp with the sampling frequency of 500 Hz, i.e., AFz, F3, F4, Fz, C3, C4, Cz, CPz, P3, P4, Pz, POz, O1, O2 and Oz, based on 10–20 international electrode system [56]. The reference is the average potential of two earlobes. This EEG acquisition paradigm is expected to cover the cortical regions highly related with the MWL variations [8,12,20,37,47]. When the experiment began, the subject sat in front of the computer where ACAMS runs and was not allowed making head or body movements. The task of ACAMS was accomplished only by using the mouse of the computer. Furthermore, the collected EEG was simultaneously visualized by the other computer. When the significant EMG artifacts were observed for a long time in the visualized EEG signals, the data collection experiment would be terminated and the data of this trial were removed. The subject was asked to rest for 20 min and begin another trial. It is noted that only in the second control condition of trial E1 we found this problem and the data of this trial were recollected.

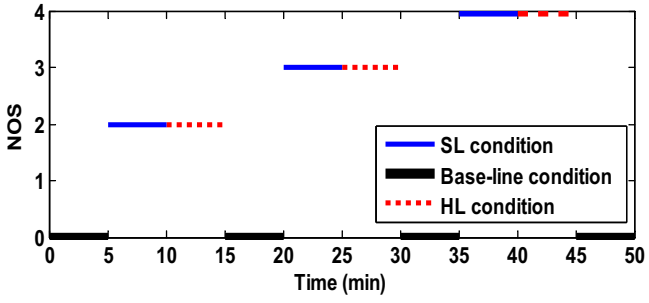

Fig. 1 – The change of control conditions in one trial.

Raw EEG data were pre-processed by a Butterworth IIR filter with the low-pass frequency of 40 Hz. The coherence method [57] was used to remove the blink artifact in the frontal EEG. Then, EEG–PSD was computed by using fast Fourier transformation with frequency resolution of 1 Hz from each 1-s clean EEG epoch. For each channel, forty frequency-domain EEG features corresponding to 1–40 Hz were extracted. After correcting outliers, the mean of each EEG feature in 5-s were calculated. Hence, The size of EEG feature set for one trial is 580×600, where 580 is the number of EEG feature vectors with the last 10-s data of each phase were omitted and 600 is the number of frequency domain features. Finally, the time courses of each feature set were standardized by subtracting the mean and dividing by the standard deviation to ensure that all features have equal significance for the subsequent analysis.

To objectively quantify the task performance of the subjects, time in range (TIR) is defined as the time ratio of the ACAMS system in the safe state during a certain time period [20,47]. TIR is computed based on the historical trajectories that were recorded by ACAMS:

$$\mathrm{TIR} = \frac{r_{O_2}(k) + r_P(k) + r_{CO_2}(k) + r_T(k)}{4}.$$

When the subsystem (O_2, P, CO_2 or T) was falling in the target range at time k, $r(k) = 1$ would be set (otherwise $r(k) = 0$). Hence, the range of TIR computed in each second is from

Table 2 – Task performance of manual condition phases quantified by TIR.

Trial	Phases with SL conditions			Phases with HL conditions		
	Phase 2	Phase 5	Phase 8	Phase 3	Phase 6	Phase 9
A1	0.93	0.91	0.80	0.79	0.74	0.59
A2	0.96	0.96	0.76	0.72	0.68	0.42
B1	0.96	0.89	0.81	0.76	0.66	0.43
B2	0.93	0.91	0.81	0.79	0.72	0.40
C1	0.97	0.92	0.84	0.76	0.69	0.55
C2	0.96	0.97	0.88	0.79	0.72	0.52
D1	0.94	0.90	0.82	0.75	0.66	0.51
D2	0.97	0.90	0.83	0.74	0.70	0.57
E1	0.98	1.00	0.96	0.87	0.85	0.71
E2	0.97	1.00	0.93	0.86	0.83	0.72
Average	0.957	0.936	0.844	0.783	0.725	0.542

zero to one. Since the goal of tasks for the subjects is to control all subsystem within the target ranges. The large TIR can represent the safety performance of ACAMS and the small TIR indicates the performance breakdown. The mean TIR of all manual condition phases are summarized in Table 2. It is shown that the order of the task difficulty of the manual condition phases from low to high is 2, 5, 8, 3, 6 and 9. In particular, TIR of phase 9 indicates the extremely poor performance, where the mean value is 0.542 and significantly lower than other phases, e.g., compared with phase 2 ($F(1, 8) = 71.52$, $p < 0.001$ with ANOVA and $W = 15$, $p < 0.05$ with directional Wilcoxon signed-rank test) and even phase 6 ($F(1, 8) = 10.4$, $p < 0.05$ with ANOVA and $W = 15$, $p < 0.05$ with directional Wilcoxon signed-rank test). On the other hand, the mean of TIR for phase 2 is close to 1. Hence, the MWL levels of one trial can be inferred as at least three classes, i.e., low (phase 1, 4, 7, 10, baseline states), normal (phase 2, good performance) and high (phase 9, poor performance).

2.3. *Identification of MWL variations*

The architecture of EEG-based MWL variation identification framework is illustrated in Fig. 2. As data preprocessing scheme is given in the previous section, the following subsections explain each of the remaining stages: EEG-based MWL feature extraction by using LLE, MWL clustering by using SVC, and binary MWL classification by using SVDD in more detail. It is noted that, SVC and SVDD can be separately used to deal with a binary MWL detection problem and can also form a hybrid approach to identifying three-class MWL.

2.3.1. *EEG-based MWL feature extraction by using LLE*

Feature selection or dimensionality reduction is quite necessary for extracting the most representative indicators to improve the reliability and interpretability of the framework since 600 EEG features are considered. This procedure could be achieved by using the expert knowledge [17], coefficient analysis with task performance [8] and principle component analysis (PCA) [8,12,37]. However, the behavior of EEG features is significantly nonlinear [8,33] while the linear projection achieved by using PCA may lose potentially important information. Meanwhile, the operator performance data is hardly available for highly automated control conditions, e.g., flight task [19] or baseline conditions in this study. To this end, LLE is applied to extract MWL indicators for several reasons. Firstly, consistent brain process related to MWL variations is reflected by EEG–PSD series with sufficient time–frequency resolution and it is assumed to form a manifold with limited dimensionality in data space. The MWL indicators can be considered as low-dimensional embeddings which best fit the high-dimensional EEG features based on *locally linear* approximation. Secondly, it is naturally suitable for dimensionality reduction of nonlinear EEG feature set since LLE could achieve *globally nonlinear* transformation of PSD vectors and the optimal information preservation is expected. At last, LLE is an unsupervised method and could fuse EEG features automatically.

For successfully implementing LLE, the smoothness of the manifold [48] is a crucial prerequisite. Meanwhile, the variation of EEG features behaves differently on multiple cortical regions. It would be thus suitable to build multiple

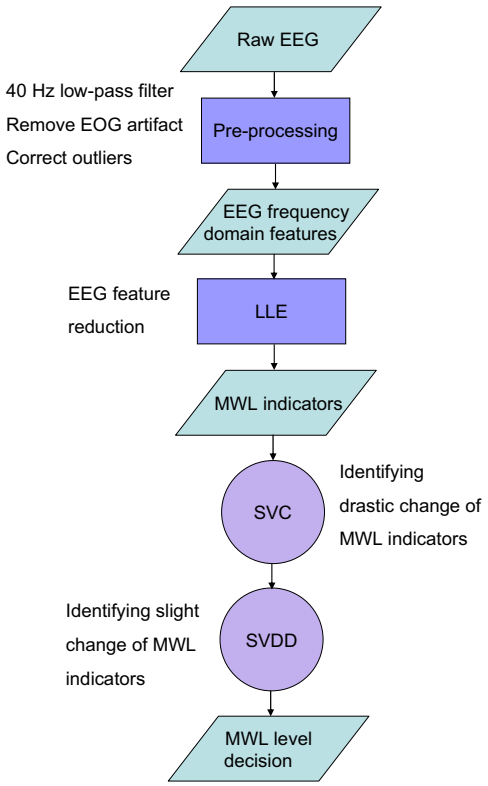

Fig. 2 – EEG-based MWL variation identification framework.

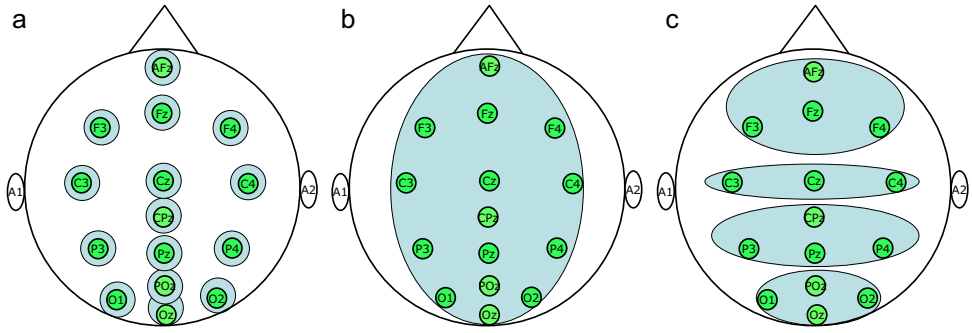

Fig. 3 – Different combinations of EEG channels on scalp for eliciting the LLE inputs: (a) grouping scheme 1, (b) grouping scheme 2, and (c) grouping scheme 3.

LLE processes to deal with a group of EEG features that has similar behaviors. To find the best way, three schemes for using EEG futures from different combinations of channels as LLE inputs are considered. Fig. 3 illustrates the three grouping schemes and they are defined as follows.

Grouping Scheme 1: each channel is separately used to build one LLE process while fifteen processes are derived in total. *Grouping Scheme 2*: all channels are used to build a single LLE process. *Grouping strategy 3*: four LLE processes are built based on four different channel groups, e.g., group 1 contains AFz, F3, F4 and Fz on the frontal region, group 2 contains C3, C4 and Cz on the central region, group 3 contains P3, P4, Pz, and CPz on the parietal region, and group 4 contains O1, O2, Oz and POz on the occipital region. It is noted that strategy 3 is inspired by the results of [8] that indicates three dipole locations of EEG sources related to mental task performance are centered in frontal, parietal and occipital regions, respectively.

In addition, two parameters for each LLE process should be selected carefully, i.e., the number of nearest neighbors K and the output dimensionality d. The nonlinear characteristic of EEG–PSD can be reflected by K while d reveals the intrinsic dimensionality of the manifold. Here, K and d are independently determined based on the smallest *reconstruction error* and the *residual variance* [58], respectively. On one hand, minimizing the reconstruction error results from the approximation of each EEG–PSD vector $\mathbf{x}_i$ and its optimal linear combination of K nearest neighbors. It is defined as:

$$\min_{w_{ij}} E = \sum_{i=1}^{N} \left| \mathbf{x}_i - \sum_{j=1}^{N} w_{ij}\mathbf{x}_j \right|^2,$$

$$\text{s.t.} \sum_{j=1}^{N} w_{ij} = 1, \forall \mathbf{x}_j \notin KNN(\mathbf{x}_i), w_{ij} = 0,$$

where w_{ij} denotes the normalized linear combination weights, $KNN(\mathbf{x}_i)$ represents the set of K nearest neighbors of $\mathbf{x}_i$ and N is the total number of EEG–PSD vectors. Optimal K corresponds the smallest min E. On the other hand, residual variance is defined as $\sigma_R^2(\mathbf{D_A}, \mathbf{D_B}) = 1 - \rho^2_{\mathbf{D_A}\mathbf{D_B}}$, where $\mathbf{D_A}$ and $\mathbf{D_B}$ are the similarity matrices (i.e., the elements are the distances between each two samples) of LLE inputs and outputs respectively and $\rho_{\mathbf{D_X}\mathbf{D_Y}}$ denotes the Bravais–Pearson correlation coefficient taken over all entries of $\mathbf{D_A}$ and $\mathbf{D_B}$. The smallest residual variance implies that the relative distances of samples are best preserved. For the grouping scheme 1, the average d summed from all groups across all subjects and trials is 38.8 with the standard deviation of 7.96. For the grouping scheme 2 and 3, the averages of summed d are 2.3 and 12.0 with the standard deviations of 0.48 and 2.79, respectively. It can be found that for all schemes the dimensionality of the LLE outputs were highly reduced compared to the original dimensionality of EEG features and the different schemes also influence the distribution of summed d. After the optimal K and d are determined, the low dimensional embeddings of EEG–PSD, defined as *MWL indicators*, are computed and ranked by using *Shannon entropy* while the ones with smooth behaviors (correspond to larger Shannon entropy) are selected for subsequent analysis [59].

2.3.2. *MWL clustering by using SVC*

Firstly, a single SVC process is applied on MWL variations detection between baseline conditions (phase 1, 4, 7 and 10) and manual conditions (phase 2, 3, 5, 6, 8 and 9). This type of binary MWL variations (denoted as case 1) would occur six times at six switch points between baseline and manual condition phases in one trial, i.e., *across phase 1–2*, *phase 3–4*, *phase 4–5*, *phase 6–7*, *phase 7–8* and *phase 9–10*. Clustering analysis is then applied on two phases of MWL indicators surrounded the switch point for binary MWL clustering. All manual conditions are defined as *normal-high* MWL level while the baseline condition is low MWL level, i.e., the labels of clusters are assigned according to control conditions.

In this study, SVC is employed based on two reasons. Firstly, using SVC is unnecessary to predetermine the number of clusters. The results of SVC vary flexibly and can be controlled by several parameters. Moreover, SVC has the capacity to deal with the overlapping of clusters by using soft clustering boundaries and thus clear clusters are expected to be recognized.

For achieving nonlinear clustering boundary, Gaussian radial basis function (RBF) kernel is adopted and it is defined as $K(\mathbf{m}_i, \mathbf{m}_j) = \exp(-\left\|\mathbf{m}_i - \mathbf{m}_j\right\|^2/\sigma^2)$, where $\mathbf{m}_i$ is the MWL indicator vector. The shape of the SVC clustering boundary is then governed by regularization parameter C and RBF width σ. In order to derive clear-cut clusters, $C \in [0.1, 0.3]$ [47] and $\sigma \in [0.2, 0.4]$ are used between different trials.

To interpret the different clusters of MWL indicators as the MWL variations, the clustering results are summarized as a *clustering matrix*. Each element of the matrix is computed via: $c_{ij} = p_{ij}/q_i$, $i = 1, 2, \ldots, n$, $j = 1, 2$, where n is the number of clusters, i denotes the cluster label, j represents the phase index, p_{ij} denotes the number of samples of each cluster within each phase and q_i is the number of samples of each cluster. Hence, the clustering matrix represents whether or not the samples of one cluster are concentrated in a single phase. If any clusters are evenly distributed in all phases, it implies the MWL variation can not be detected and vice versa. Moreover, the *detection threshold* was defined to control the overlapping of the clusters. The values of the detection threshold within a finite set {0.1, 0.2, . . ., 0.5} are examined separately. Each value in the set represents the upper bound of the percentage of samples that are wrongly clustered, e.g., the samples in phase 1 are clustered into cluster 2. Namely, the detection threshold is required to be determined not too small or too large for controlling the sensitivity of recognizing MWL variations [59]. In subsequent analysis, detection threshold is empirically set to 0.3 by exploring all possible values in the parameter set. In this case, MWL variation would be detected only if 70% samples of each cluster are concentrated in a single phase. In particular, only clusters that contain more than 10% samples are considered. It is because that the samples located near the switch point of the two successive phases are considered as the transient state between two MWL levels. In this case, the SVC approach may recognize them as a new cluster with few samples (4–8% of two-phase data) and it is difficult to accurately interpret the corresponding MWL level of these samples.

2.3.3. *Binary MWL classification by using SVDD*

SVDD is utilized to design auxiliary binary classifiers for identifying MWL variation when MWL indicators slightly vary. SVDD is a typical "one-class" classifier. The fundamental concept of SVDD is to use a smallest enclosed hypersphere to cover all the target-class samples while the non-target classes can be refused. This mechanism could be quite beneficial when low or normal MWL level is considered as the target class. In this case, MWL indicator vectors of high MWL level that represent more serious consequences can be identified with higher accuracy.

The reliability of SVDD classifier is firstly assessed by a binary MWL classification problem (denoted as case 2). In this case, MWL indicators of phase 2 or phase 2 and 5 are defined as class 1 (normal MWL) and phase 9 is defined as class 2 (high MWL). The performance of SVDD classifier is evaluated based on the training and testing paradigm, i.e., evenly separating the EEG feature set into two subsets and class 1 of one subset is used for training and the other subset is used for testing. In this case, MWL indicators should be estimated by using a nonlinear model since LLE could not generate an explicit mapping (least square support vector regression is adopted [60]). It is noted that samples in the training sets that lead to the non-smooth detection boundary are eliminated by removing the boundary support vectors. Finally, false rejection rate (FRR, type I error, misclassifying class 1 as class 2) and false acceptance rate (FAR, type II error, misclassifying class 2 as class 1) are used to evaluate the classification performance.

2.3.4. *Three-class MWL recognition by using SVC–SVDD hybrid approach*

When MWL indicators slightly vary, clear clusters cannot be yielded because of the high degree of overlapping. To this end, adopting an auxiliary classifier for further recognizing the blurred cluster is reasonable. For the purpose of increasing the identification accuracy on high MWL class, SVDD is used to build a hybrid SVC–SVDD approach. Considering both of case 1 and 2, a three-class MWL recognition problem can be inferred (denoted as case 3), i.e., low, normal, and high. In this case, SVC is first applied to identify the drastic changes of MWL indicators and the clear-cut cluster is derived. Then, SVDD is utilized to classify the additional two MWL levels that within the overlapped cluster. It is noted that there are three possibilities of the cascade mode between SVC and SVDD (Fig. 4). The type of cascade mode is determined by the class label of the clear-cut cluster identified by SVC, where the training class of SVDD is low or normal MWL to ensure the classification accuracy on high MWL class. And this label is assigned by a typical MWL indicator that has positive correlation with task difficulty. When one of samples in the identified cluster has the highest (or lowest) value of the typical MWL indicator compared with other samples, it is a high (or low) MWL cluster otherwise it is a normal MWL cluster. The overall identification accuracy is then evaluated based on the subset of each trial that contains one baseline phase (low MWL, class 1), phase 2 (normal MWL, class 2) and phase 9 (high MWL, class 3).

3. Results

3.1. *Extract EEG markers of MWL*

For each grouping scheme, 2–8 MWL indicators are elicited by LLE and selected based on Shannon entropy. In particular, two best MWL indicators are selected for each trial according to scheme 3, which show the highest clustering performance (the performance comparison is made in the next subsection). MWL indicators extracted from a representative trial (C1) are illustrated in Fig. 5. It is clearly shown that the time courses of all indicators are correlated with the change of the task difficulty. In particular, a time series represented the change of the control conditions was created according to NOS, which has the equal length with the MWL indicator. Then, the Bravais–Pearson correlation coefficient (denoted by r) was computed between them. Consequently, for the MWL indicator in the first row and the second row, r is equal to 0.4324 and 0.8776, respectively. The first row of the figure shows that the MWL indicator of the frontal scalp (denoted as MWL indicator 1 of trial C1) is highly positively correlated ($r = 0.6$) with all θ power of corresponding channels (F3, F4, Fz and AFz). Since this MWL indicator clearly increase with the task difficulty, the power of frontal θ band has the same property. The second row represents a typical MWL indicator of occipital cortical region (denoted as MWL indicator 2 of trial C1). It obviously increases with high level of task difficulty. Meanwhile, it is highly correlated with β (13–32 Hz) and γ (33–40 Hz) power of occipital channels (O1, O2, Oz and POz). Table 3 summarizes the highly correlated frequency band with two best MWL indicators of corresponding cortical regions extracted by

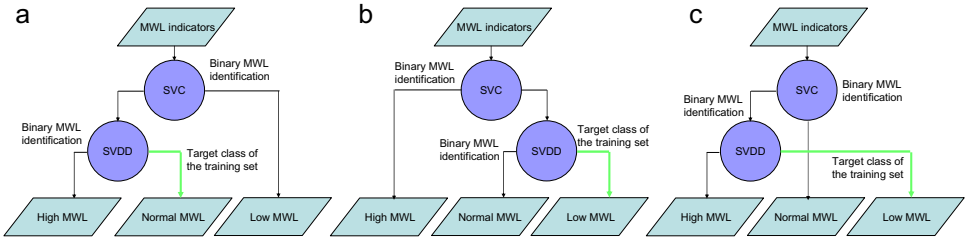

Fig. 4 – Three possibilities of cascade mode between SVC and SVDD: clear-cut cluster identified by using SVC is (a) low, (b) high or (c) normal MWL.

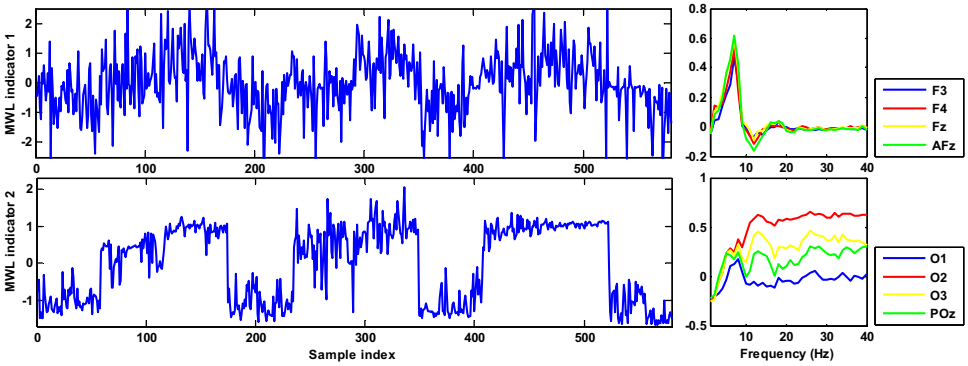

Fig. 5 – Two MWL indicators of trial C1 extracted by using grouping scheme 3. On the left column, the first row is one indicator extracted from frontal scalp, the second row is from occipital scalp. The right column shows the linear correlation coefficient between the MWL indicator and EEG-PSD across different frequency band of corresponding channels.

using grouping scheme 3. From the table, power of θ band is highly correlated with frontal MWL indicator for trial B1, C1 and C2. Power of α band is highly correlated with central MWL indicator for trial A1 and A2. Power of β and γ band is highly correlated with occipital MWL indicator for all trials.

3.2. *SVC-based MWL clustering results*

To deal with the binary MWL identification problem of case 1, a single SVC process is applied on MWL indicators. The clustering results of trial (C1) are shown in Fig. 6. Two MWL indicators corresponding to the frontal and occipital cortical regions (see in Section 3.1) were adopted. For each subfigure, two clear clusters can be recognized, which indicates the transition between binary MWL states at the switch point. Black circles are the boundary support vectors that located near the boundaries of clusters. When boundary support vectors are eliminated, the cores of clusters can be easily recognized. In addition, the labels of clusters can be assigned based on a typical MWL indicator 2 which is positively correlated with the task difficulty. Hence, the cluster located at the top region of data space is determined as the normal-high MWL (e.g., cluster 2 in Fig. 6(a)) and the lower one is low MWL (e.g., cluster 1 in Fig. 6(a)).

Table 3 – Highly correlated frequency band with two best MWL indicators of corresponding cortical regions extracted by using grouping scheme 3.

Trial	MWL indicator 1	MWL indicator 2
A1	Central, α	Occipital, α, β, γ
A2	Central, α	Occipital, β, γ
B1	Frontal, α	Occipital, γ
B2	Frontal, θ	Occipital, β, γ
C1	Frontal, θ	Occipital, β, γ
C2	Frontal, θ	Occipital, β, γ
D1	Parietal, θ, β	Occipital, α, β, γ
D2	Occipital, β, γ	Occipital, β, γ
E1	Central, θ, α, β	Occipital, θ, α, β
E2	Central, β, γ	Occipital, β, γ

Table 4 summarizes the all clustering matrixes of trial C1. It shows MWL indicator vectors that belong to the same cluster are more likely located in the same phase. At the first switch point, 81% MWL indicator vectors of the cluster 1 are located in the phase 1 and 100% points of cluster 2 are located in the phase 2. For the remaining switch points, the clustering accuracies are even higher. In particular, for switch point across phase 3–4, 7–8 and 9–10, the MWL indicator vectors are perfectly clustered. In this case, it can be identified that MWL levels alternatively change from normal-high to low and low to normal-high between two clear clusters.

Table 5 summarizes the binary MWL detection results for all trials with the threshold of 0.3 and grouping scheme 3. In this case, binary MWL transition is detected if more than 70% of MWL indicator vectors are correctly clustered. From the table, the average detection rate can be achieved to 0.75 regarding all switching points and trials. The relatively high detection rates are found in trials of subject A, C, D and E (67–100% MWL transitions are detected) while the lower ones are in both trials of subject B (25% MWL transitions are detected). The potential reason is that the quality of MWL indicators extracted by using LLE is also individually dependent

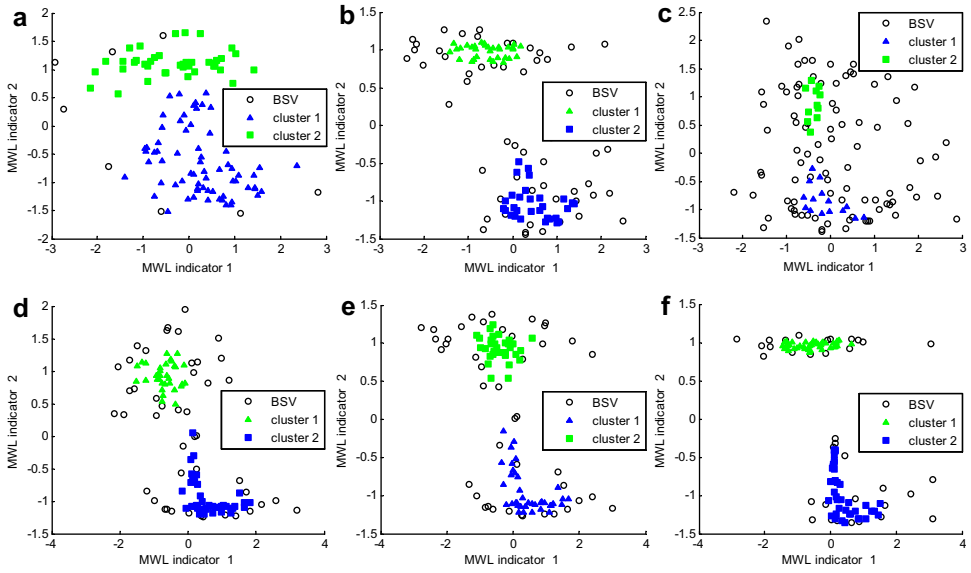

Fig. 6 – Clustering results of trial C1 across phase 1–2 (a), phase 3–4 (b), phase 4–5 (c), phase 6–7 (d), phase 7–8 (e) and phase 9–10 (f). The blue-colored marker represents the low MWL level and the green-colored marker represents the normal-high MWL level. "BSV" represents boundary support vectors. (For interpretation of the references to colour in this figure legend, the reader is referred to the web version of this article.)

[61–63]. Moreover, the MWL transition at the first switch point cannot be well detected for both trials of subject A and it indicates the mental task with low difficulty level may not lead to the sufficiently large distance between clusters.

For the comparing purpose, Table 6 summarizes the mean detection rate averaged from ten trials at six switch points with different implementations. On one hand, the results of three grouping schemes for extracting MWL indicators by using LLE are shown. With SVC subsequently employed, it is denoted as LLE–SVC. One observation is that the detection rate at switch point 4–6 across all strategies is significantly higher than those of switch point 1–3 ($F(1, 16) = 16.11$, $p < 0.01$ with ANOVA and $W = 36$, $p < 0.01$ with Wilcoxon signed-rank test). The underlying reason is that the MWL indicators drastically change from baseline-condition to manual-condition phases with high task difficulty, which leads to the far

Table 4 – Clustering matrixes across six switch points of trial C1.

	Cluster 1	Cluster 2		Cluster 1	Cluster 2
Phase 1	0.81	0.00	Phase 6	1.00	0.03
Phase 2	0.19	1.00	Phase 7	0.00	0.97
Phase 3	1.00	0.00	Phase 7	1.00	0.00
Phase 4	0.00	1.00	Phase 8	0.00	1.00
Phase 4	0.87	0.00	Phase 9	1.00	0.00
Phase 5	0.13	1.00	Phase 10	0.00	1.00

Table 5 – Detection results of binary MWL variation between baseline-condition (low MWL) and manual condition phases (normal-high MWL) with grouping scheme 3 and threshold = 0.3, SP denotes the switch point (from 1 to 6), "1" (or "0") represents MWL variation is detected (or not). DR1 and DR2 are the detection rates averaged on each trial and each switch point, respectively.

Trials	SP1	SP2	SP3	SP4	SP5	SP6	DR1
A1	0	1	1	1	1	1	0.833
A2	0	1	1	1	1	1	0.833
B1	1	0	0	0	0	0	0.17
B2	1	0	0	0	0	1	0.33
C1	1	1	1	1	1	1	1.00
C2	0	1	1	1	1	1	0.83
D1	0	1	1	1	1	1	0.83
D2	1	1	1	1	1	1	1.00
E1	1	1	1	1	1	1	1.00
E2	1	0	0	1	1	1	0.67
DR2	0.60	0.70	0.70	0.80	0.80	0.90	0.75

Table 6 – Mean detection rate for binary MWL variations (averaged from 10 trials) between baseline-condition and manual-condition phases with different implementations. Results of SVC analysis based on MWL indicators extracted by using LLE corresponding to different grouping schemes (denoted as LLE-SVC, scheme 1 to 3) compared with PCA-KCM clustering analysis (100 iterations, CPV = 0.9, $k = 2$) are presented. SP denotes index of the switch point (from 1 to 6) and the highest value of each row is in bold (for the standard deviation "std" is the smallest value).

SP	LLE-SVC			PCA–KMC
	Scheme 1	Scheme 2	Scheme 3	$k = 2$
1	0.2	0.4	**0.6**	0.4
2	0.7	0.4	**0.7**	0.4
3	0.7	0.6	**0.7**	0.5
4	0.7	**0.9**	0.8	0.4
5	0.7	**0.9**	0.8	0.8
6	0.8	0.9	**0.9**	0.7
Average	0.63	0.68	**0.75**	0.58
Std	0.216	0.248	**0.105**	0.175

distance between clusters. On the other hand, the detection rate derived from a classical clustering framework combined of PCA and *K*-means clustering (KMC) is examined (denoted as PCA–KMC) [64]. It is noted that the existing works [9] have successfully applied PCA on the EEG powers for feature reduction under the context of MWL/performance assessment. In recent works [8,12], PCA was separately applied or combined with the independent component analysis technique for EEG spectrum analysis. In particular, when the driving task is considered, EEG features after PCA mapping show significant relevance to the task performance. On one hand, only certain frequency contents of the EEG signal significantly change with the increase of degree of mental workload. If the entire EEG spectra are used as the input features of a classifier, the issue of curse of the dimensionality can significantly degrade the classification performance. In this case, the role of use of PCA is to find the covariance direction with most salient variation in the EEG feature space and hence adopt a few principal components as the extracted EEG-power features. Although the non-stationarity characteristics of EEG signals may cause a slight reduction of classification accuracy, the use of PCA method is viable, especially when only a few discrete levels of mental workload are considered for the pattern recognition problem, because the overly higher dimensionality of EEG-related features may affect the performance of the machine-learning-based classifiers more seriously than the signal nonlinearity property. On the other hand, the goal of using LLE instead of PCA is to examine the efficacy of the nonlinear method. As PCA was traditionally used in assessing mental workload based on the electrophysiological features, it is necessary to compare the proposed method with it. The standard parameter settings of PCA are considered, i.e., adopting cumulative percent variance (CPV) of 0.9 to select the representative principle components while the number of clusters for KMC is set to 2 for binary clustering and iteration time is 100. When scheme 3 is utilized, LLE–SVC is significantly superior to PCA–KMC ($F(1, 10) = 6.76$, $p < 0.05$ with ANOVA and $W = 15$, $p < 0.05$ with Wilcoxon signed-rank test). However, for scheme 1, the improvement is not significant ($F(1, 10) = 0.78$, $p = 0.39$ with ANOVA and $W = 10$, $p = 0.31$ with Wilcoxon signed-rank test) and it is same for scheme 2 ($F(1, 10) = 1.46$, $p = 0.25$ with ANOVA and $W = 11$, $p = 0.11$ with Wilcoxon signed-rank test). It is noted that PCA–KMC scheme always requires predetermining the number of clusters while SVC is unnecessary. Hence, SVC has the capacity to find the more natural clusters with different characteristics of MWL indicators across subjects. In this way, the binary MWL variations between low and normal-high can be well identified.

3.3. *SVDD-based MWL classification results*

For the binary MWL identification problem of case 2, SVDD is employed for separating these two states that may have higher overlapping of MWL indicators (can be inferred from Fig. 5). Considering the highest clustering performance, MWL indicators are all extracted based on grouping scheme 3. The training and testing process of a single trial (A1) is illustrated in Fig. 7. Firstly, a hypersphere is trained with MWL indicator vectors of normal MWL with small *C* adopted ($C \in [0.05, 0.2]$) and the boundary support vectors are recognized. Then, a new SVDD model provides more flexible boundary with large *C* adopted ($C \in [0.8, 1]$) and the boundary support vectors are removed. The reason for adopting this procedure is that these samples often lead to the non-smooth detection boundary, which indicates the low generalization capacity of the classifier. To alleviate this overfitting problem and recognize the candidate boundary support vectors, the regularization parameter *C* of SVDD model is carefully selected from 0.05 to 0.2. In this case, several boundary support vectors can be automatically identified by the SVDD algorithm (the corresponding Lagrange multiplier of the sample is larger than the regularization parameter [50]). When SVDD model is applied on the testing set, the MWL indicator vectors of high MWL (or normal MWL) almost lie outside (or inside) the hypersphere. Hence, a binary classification between normal and high MWL can be achieved.

Detailed MWL classification results of three representative trials (A1, C1 and D1) are illustrated in Fig. 8, where the distance of each testing sample to the center of the hypersphere in kernel space is shown. If the distance is larger (or smaller) than the hypersphere radius, it would be determined as a high (or normal) MWL sample. It is noted that the testing sets are built by two forms to evaluated the performance of SVDD model, i.e., using phase 2, 5, 9 (denoted as testing set 1) and phase 2 and 9 (denoted as testing set 2), where only samples in phase 9 are denoted as high MWL. From the figure, most of the high MWL samples are located above the detection boundary and the normal MWL samples are below it.

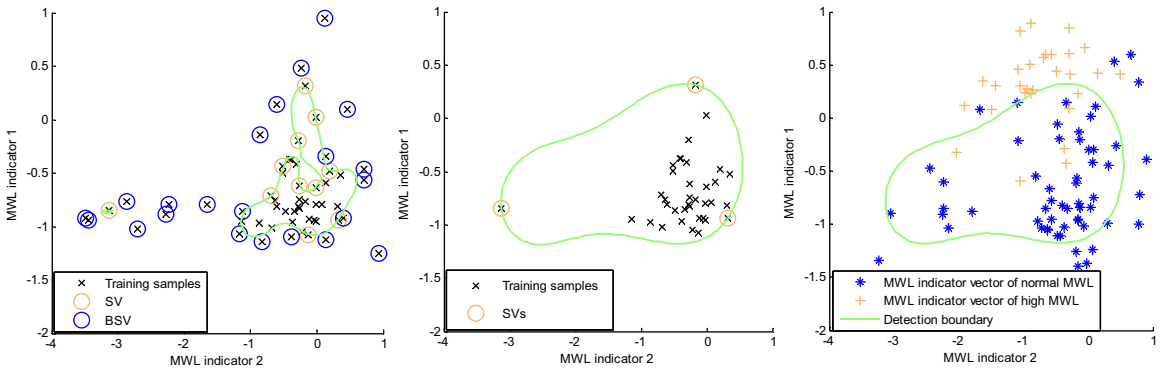

Fig. 7 – Training and testing processes of trial A1 by using SVDD for binary MWL identification: (1) identifying and eliminating boundary support vectors "BSV" (left), (2) building SVDD model with flexible detection boundary (middle), (3) MWL identification on testing set (right). "SV" represents support vectors.

The classification results for all trials are summarized in Table 7, where FRR and FAR are computed. On one hand, the elicited FAR is significantly lower than FRR ($F(1, 38) = 5.33$, $p < 0.05$ with ANOVA). It is reasonable because that the smallest hypersphere which surrounds normal samples are always considered. Hence, the model is more sensitive for detecting high MWL samples at the cost of the increasing false alarm events. Since false acceptance events are considered as more serious consequences, the lower FAR could be beneficial for safety-critical environment. Additionally, for both results of testing set 1 and 2, the acceptable accuracy are achieved, which indicates the normal and high levels of MWL can be well classified.

For comparing purpose, SVDD is also examined when PCA scheme is adopted for EEG–PSD feature fusion (denoted as PCA–SVDD scheme). Meanwhile, Hotelling's T^2 statistic and the squared prediction error (SPE) of the multivariate control chart technique [65] have been also computed based on PCA (denoted as PCA-T^2 and PCA–SPE scheme, respectively). The application of PCA-T^2 scheme for the similar purpose has been

Table 7 – Binary MWL classification results (case 2, normal and high MWL) on two forms of the testing sets (testing set 1 and 2) by using SVDD, FRR (type I error) and FAR (type II error) are presented.

Trial	Testing set 1		Testing set 2	
	FRR	FAR	FRR	FAR
A1	0.241	0.207	0.276	0.069
A2	0.483	0.345	0.552	0.345
B1	0.241	0.172	0.241	0.138
B2	0.483	0.379	0.655	0.103
C1	0.121	0.069	0.069	0.069
C2	0.138	0.069	0.000	0.000
D1	0.017	0.000	0.138	0.000
D2	0.310	0.000	0.103	0.000
E1	0.328	0.310	0.310	0.172
E2	0.069	0.000	0.036	0.000
Average	0.228	0.179	0.207	0.103

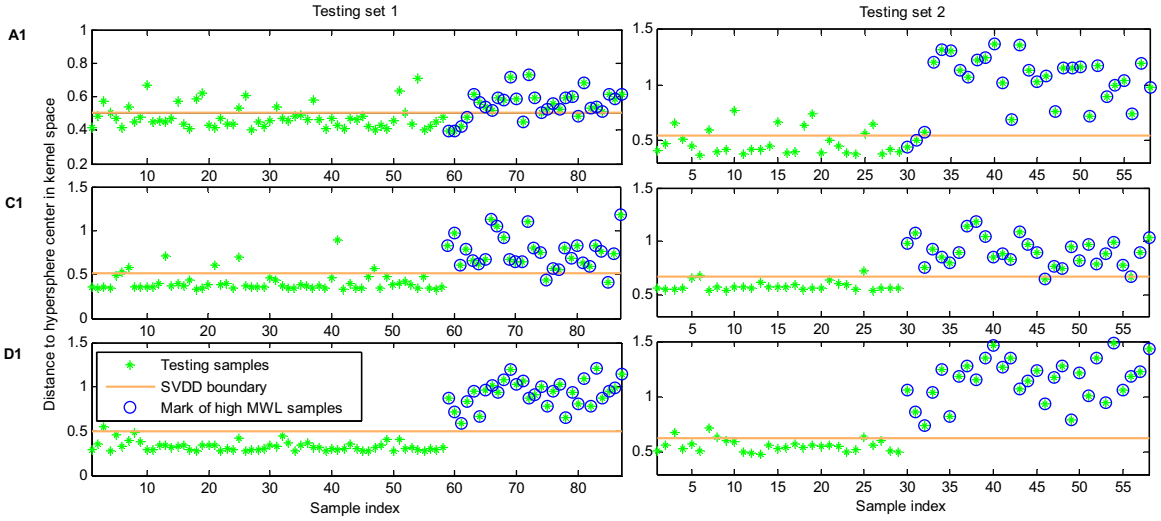

Fig. 8 – Binary (normal and high) MWL classification results on testing sets built by MWL indicator vectors of phase 2, 5, 9 (left column) and phase 2 and 9 (right column), the distance of each vector from the center of hypersphere of SVDD model in kernel space on trial A1 (top), C1 (middle), and D1 (bottom) are represented.

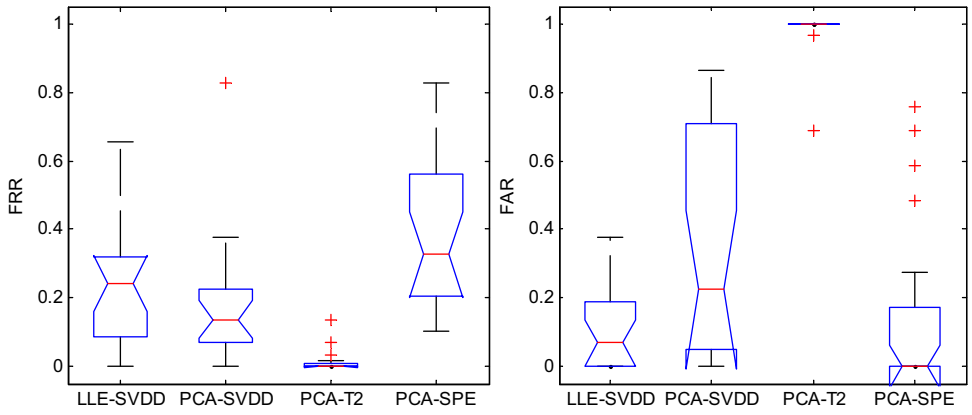

Fig. 9 – Classification accuracy represented by FRR and FAR for binary MWL classification of case 2 (normal and high MWL) based on LLE–SVDD, PCA–SVDD, PCA-T^2 and PCA–SPE schemes.

already explored [12]. With CPV = 0.9, the upper confidence limit of statistic in PCA-T^2 and PCA–SPE schemes is determined by the confidence level of 0.95. This limit is defined as the detection boundary for high MWL samples. The classification accuracy elicited from the three methods under the same training and testing framework are compared with the results in Table 7 (denoted as LLE–SVDD) and the boxplot of FRR and FAR is shown in Fig. 9. The statistical analysis for comparing classification performance by using ANOVA is performed. From the figure, both FRR and FAR show significant difference ($F(3, 76) = 15.75$, $p < 0.001$ and $F(3, 76) = 61.57$, $p < 0.001$) while the results from PCA-T^2 are meaningless since its FAR is unacceptable high. Considering FRR, PCA–SVDD achieves the lowest mean value, which is significantly lower than that of PCA–SPE ($F(1, 38) = 10.68$, $p < 0.005$) and not significant compared with LLE–SVDD ($F(1, 38) = 1.22$, $p = 0.276$). Meanwhile, considering FAR, PCA–SPE achieves the lowest mean value and it is significantly lower than PCA–SVDD ($F(1, 38) = 4.59$, $p < 0.05$) while not significant compared with LLE–SVDD scheme ($F(1, 38) = 0.16$, $p = 0.692$. On the other hand, LLE–SVDD provides a significant lower FRR than PCA–SPE ($F(1, 38) = 5.25$, $p < 0.05$) as well as a significant lower FAR than PCA–SVDD ($F(1, 38) = 7.91$, $p < 0.01$). Hence, LLE–SVDD shows the most balance performance on FRR and FAR and it could achieve the comparable accuracy with methods that show the lowest FRR and FAR.

3.4. *SVC–SVDD hybrid approach based three-class MWL recognition results*

The hybrid SVC–SVDD approach is applied for three-class MWL identification of case 3. Fig. 10 shows the results of three representative trials (A1, C1 and D1). The first observation is that one of the clusters lies relatively far away from other samples and can be easily identified by SVC model while the remaining cluster is divided into two parts by the boundary of subsequent SVDD model. Hence, three groups of MWL

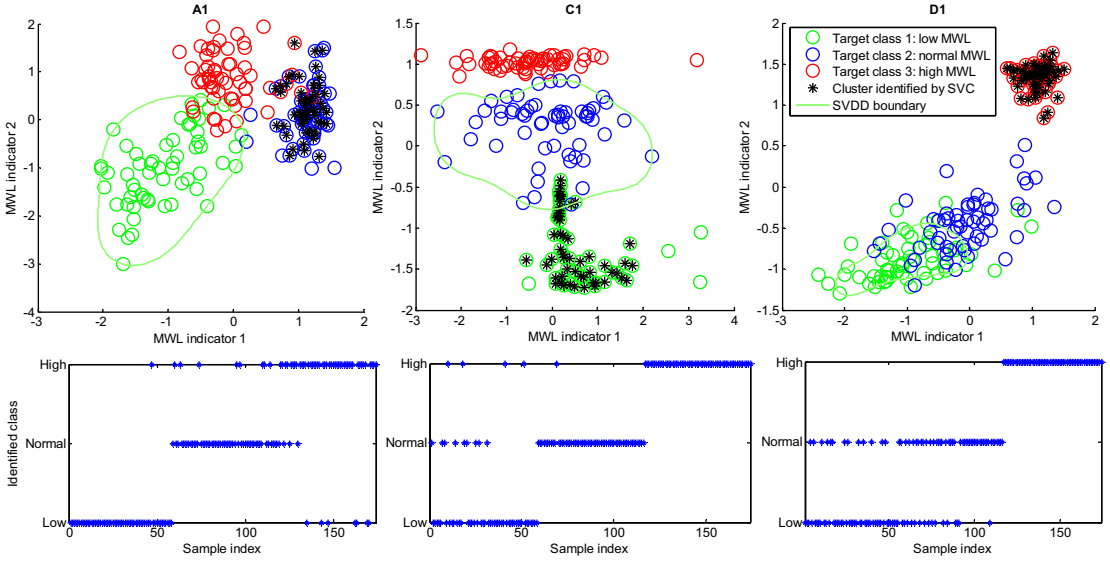

Fig. 10 – Three-class MWL (low, normal and high) identification by using hybrid SVC–SVDD approach on MWL indicators. The results of trial A1 (left column), C1 (middle column) and D1 (right column) are given. The first row shows the predetermined class label (1–3: low, normal and high MWL), the cluster identified by SVC and the SVDD boundary for classifying blurred cluster. The second row shows the identified class by SVC–SVDD approach.

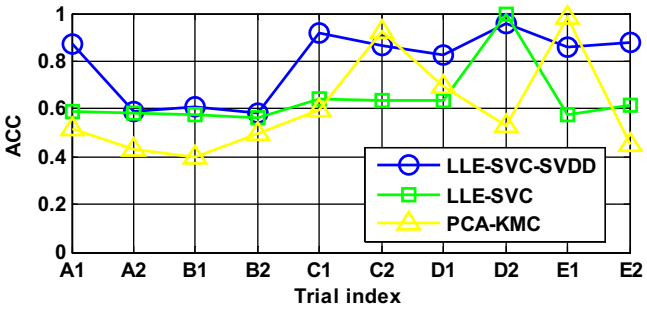

Fig. 11 – Three-class MWL identification accuracy (ACC) elicited by using SVC–SVDD hybrid approach and single SVC model on MWL indicators (denoted as LLE–SVC–SVDD and LLE–SVC) as well as PCA–KMC approach (with CPV = 0.9, $k = 3$, 100 iterations).

indicator vectors are determined. Then, the class labels are assigned based on the typical MWL indicator (MWL indicator 2) that has high positive correlation with the task difficulty. For instance, when all clusters are projected on the axis of MWL indicator 2, the center (mean value) of the high, normal and low MWL clusters always lay in the top, middle and bottom place. The second observation is that the class label of the first identified cluster may vary. Namely, for trial A1, this cluster represents normal MWL while for C1 and D1 are low and high MWL, respectively. Hence, the different cascade mode between SVC and SVDD is activated and training samples of one target class (e.g., low or normal MWL) are utilized to build the SVDD boundary. According to this procedure, the final MWL identification results are elicited (the second row of Fig. 10). The identification accuracy is computed based on the predetermined class labels, i.e., low MWL: baseline condition phase (sample index 1–58); Normal MWL: manual condition phase 2 (sample index 59–116); high MWL: manual condition phase 9 (sample index 117–174).

The accuracy of identifying three-class MWL levels (denoted as ACC) elicited by using SVC–SVDD hybrid approach on MWL indicators (denoted as LLE–SVC–SVDD) are compared with other two implementations on same EEG feature sets (Fig. 11). In the first implementation, SVC–SVDD model is replaced by a single SVC model (LLE–SVC). In the other case, PCA–KMC approach is applied again (with CPV = 0.9, $k = 3$, and 100 iterations) while the class labels are empirically assigned. It can be found that LLE–SVC–SVDD approach achieves the higher ACC (mean value is 0.7954) than LLE–SVC (mean value is 0.6407) and PCA–KMC (mean value is 0.6022). The underlying reason is that single SVC process as well as PCA–KMC approach could hardly recognize more than two meaningful clusters while about 60% samples are determined as the same cluster. Namely, in some cases, clustering approaches cannot reliably divide clusters between high and normal MWL. Moreover, the results of PCA–KMC approach are difficult to interpret and visualize because dimensionality of extracted principle components is still high. According to the ACC computed on all trials, LLE–SVC–SVDD significantly outperforms LLE–SVC ($F(1, 18) = 6.49$, $p < 0.05$ with ANOVA and $W = 47$, $p < 0.05$ with Wilcoxon signed-rank test) and PCA–KMC approach ($F(1, 18) = 5.98$, $p < 0.05$ with ANOVA and $W = 47$, $p < 0.05$ with Wilcoxon signed-rank test).

4. Discussions

The results of the presented study show the capacity of EEG-based hybrid clustering-classification approach which contains LLE–SVC, LLE–SVDD and LLE–SVC–SVDD schemes for coping with MWL variation identification problem. Since one subject's data were removed from the study due to the data acquisition problem, it is no doubt the number of subject is relatively lower than the related works. Despite this weakness, for each subject two trials of the experiment were performed and for each trial 50 min data were collected. Thus, enough psychophysiological data samples can be extracted for statistical analysis. Moreover, similar results across subjects were observed, which has validated the effectiveness of the proposed approach.

On one hand, LLE could automatically extract the representative MWL indicators with proper grouping scheme according to the spatial distribution of channels, e.g., frontal θ activity which is known in many cognitive tasks that require attention and working memory [20] and the suppression of parietal α activity [27]. Meanwhile, the beta rhythm has been also observed in a driving task [8]. On the other hand, when all channels are adopted as one group, the clustering performance (represented by the detection rate) decreases. The potential reason is that EEG features, which were differently varying based on the cortical regions, lead to the discontinuity of the manifold formed in the high dimensional data space. It would essentially undermine the accuracy for the locally linear approximation with LLE. Meanwhile, when the single channel is used as one group, the corresponding MWL indicators are duplicated and difficult to find the most representative ones. Hence, with proper grouping scheme of EEG channels, low-dimensional MWL indicators which are easily visualized and interpreted can be derived from high dimensional EEG–PSD features.

With LLE–SVC scheme, clear-cut clusters for the successive two-phase data could be derived. The corresponding cluster matrix can represent the transition of the binary levels of MWL between baseline-condition and manual-condition phases. It shows the clustering approaches can also lead to an effective way for interpreting EEG features related to MWL variations. However, a single LLE–SVC procedure cannot well detect slight change of MWL indicators when a three-class MWL identification problem is considered. The potential reason is that the overlapping of extracted MWL indicators is severe so that contours of the hypersphere of SVC cannot be spilt to define a cluster.

With LLE–SVDD framework implemented, MWL indicators corresponding to normal MWL is used to describe a "boundary" of the safety operator function state while the risky state with low operator performance could be refused. This approach significantly outperforms the PCA-based methods. The reason may lie in that the distribution assumptions of PCA (i.e., independently identically Gaussian distributed) cannot be fully satisfied with limited training samples adopted and it could only fuse EEG features in a linear way. Meanwhile, these

assumptions are not necessary for applying LLE–SVDD, where the non-parametric nonlinear procedure (LLE approximation) as well as the soft and flexible detection boundaries (achieved by the kernel function) could be adaptive for any types of the data distribution. Moreover, LLE–SVDD could achieve higher FAR than FRR and it could be beneficial for the application of safety-critical human–machine system.

Finally, taking advantages of both LLE–SVC and LLE–SVDD, LLE–SVC–SVDD hybrid approach is applied for three-class MWL identification problem. The clear-cut cluster is first recognized and SVDD could separate the remaining blurred cluster. Meanwhile, the accuracy of LLE–SVC–SVDD is significantly higher than unsupervised frameworks of LLE–SVC and PCA–KMC. Hence, it can potentially contribute to the application of MWL monitoring as well as adaptive aiding since much less training samples are required for building the psychophysiological-data-driven decision system.

It should be pointed out that the temporal effect would be also reflected by the EEG powers when the subject is sustained to be wakeful for quite a long time. For instance, it has been observed that EEG power density in θ frequency band progressively increased after the subject was being awake for at most 40 h [66]. Moreover, the fatigue accumulation and the drowsiness would happen when the operator performs the monotonous driving task for hours. The driver's fatigue can be represented by the variations of EEG powers in θ, α and β bands [67]. Since these EEG power features are also salient for MWL changes, it is no doubt that the fatigue accumulation will also influence the change of the MWL indicators in the presented study. Under the context of the experimental settings of ACAMS, it is reasonable to consider the time effect as a secondary factor for the change of EEG powers. The first reason is that the overall time duration of one trial experiment is only 50 min and it would not lead to the significant fatigue. Furthermore, baseline conditions occurred alternatively and it could help the subject recover somewhat from the stress generated by tasks. In addition, the drowsiness can be alleviated when the subject performed a series of short-time tasks with different difficulties. However, exploring the interaction between the variations of MWL and fatigue by using quantitative methods can be quite beneficial for understand the origin of the operator's performance breakdown and it is potentially an interesting and promising topic in the future work.

There are certainly several limitations to be addressed in the presented study. Firstly, the time delay effects possibly present in the LLE–SVC–SVDD framework should be taken into consideration especially when the EEG features are sampled at a faster rate. Secondly, a computer-based quantitative and automatic, rather than empirical, procedure to determine the optimal parameters of SVDD should be developed. Considering the EEG feature reduction techniques, other nonlinear dimensional reduction techniques, e.g., kernel principal component analysis, isomap, diffusion maps, maximum variance unfolding, summon mapping, Laplacian eigenmaps, locally linear coordination [68], are also promising and rarely explored in the literature. It is also noted that some of these methods are need to be adjusted for adapting the specific applications [69]. Moreover, ECG related features that are also closely related to the activity of the autonomous nervous system, e.g., heart rate and heart rate variability, should be taken into account and combined with EEG features since it has been found that the power of the mid-frequency band (0.04–0.14 Hz) of HRV decreases with the increase of the cognitive task difficulty [70–72]. In addition, the number of subjects is relatively low compared to the related works [33] and somehow limited the significance of the results. Therefore, the dataset contains sufficient subjects should be collected under the future experiment. Last but not least, considering the real-time MWL assessment problem, an obvious limitation of the present study lies in that our data processing were conducted offline. For the online application, standardizing EEG features separately for different trials is no longer available and need to be modified. The hardware implementation and the computational efficiency of the classification methods also need to be optimized and examined. In our future work, the multimodal approach [34–36] that combines EEG with different portable neuroimaging methods should be also considered since it shows promising usability in real-time human system interactions.

5. Conclusions

In this paper, an EEG-data-based high-risk MWL detection framework by combining unsupervised and supervised learning has been proposed and validated based on the most typical EEG markers (MWL indicators) extracted by use of LLE algorithm. It is shown that the high-dimensional frequency-domain EEG features can be well represented by their low-dimensional embeddings. The LLE–SVC–SVDD hybrid framework was successfully applied to MWL monitoring based solely on the measured psychophysiological data. Despite some limitations, the presented study shows a promising way to find EEG markers related to the MWL variation which can be effectively recognized by the proper classifiers. In our future plan, we would develop reliable real-time MWL assessment method with an aim to avoid/mitigate the occurrence of risky operator functional states which may result in unacceptable decrement even breakdown of human performance.

Conflict of interest statement

Zhong Yin and Jianhua Zhang declare no conflict of interest.

Acknowledgments

The authors would like to thank the developers of the ACAMS software which was used in our experiments. The work was supported by the National Natural Science Foundation of China under Grant No. 61075070 and Key Grant No. 11232005. The authors wish to thank Prof. Dr.-Ing. Joerg Raisch (Control Systems Group of Technical University of Berlin, Germany) for his support and helpful comments on the draft version of this paper. The comments of Mr. Yuxin Ma are also gratefully acknowledged.

REFERENCES

[1] E.A. Byrne, R. Parasuraman, Psychophysiology and adaptive automation, Biol. Psychol. 42 (1996) 249–268.

[2] G.R.J. Hockey, A.W.K. Gaillard, O. Burov, Operator functional state: the assessment and prediction of human performance degradation in complex tasks, 2003, pp. 8–13 (Amsterdam, the Netherlands).

[3] D.B. Kaber, C.M. Perry, N. Segall, C.K. McClernon, L.J. Prinzel, Situation awareness implications of adaptive automation for information processing in an air traffic control-related task, Int. J. Ind. Ergon. 36 (2006) 447–462.

[4] O. Tonet, M. Marinelli, L. Citi, P.M. Rossini, L. Rossini, G. Megali, P. Dario, Defining brain-machine interface applications by matching interface performance with device requirements, J. Neurosci. Methods 167 (2008) 91–104.

[5] G.F. Wilson, C.A. Russell, Performance enhancement in an uninhabited air vehicle task using psychophysiologically determined adaptive aiding, Hum. Fact. 49 (2007) 1005–1018.

[6] S.K.L. Lal, A. Craig, A critical review of the psychophysiology of driver fatigue, Biol. Psychol. 55 (2001) 173–194.

[7] C.T. Lin, K.C. Huang, C.F. Chao, J.A. Chen, T.W. Chiu, L.W. Ko, T.P. Jung, Tonic and phasic EEG and behavioral changes induced by arousing feedback, NeuroImage 52 (2010) 633–642.

[8] S.W. Chuang, L.W. Ko, Y.P. Lin, R.S. Huang, T.P. Jung, C.T. Lin, Co-modulatory spectral changes in independent brain processes are correlated with task performance, NeuroImage 62 (2012) 1469–1477.

[9] C.T. Lin, R.C. Wu, T.P. Jung, S.F. Liang, T.Y. Huang, Estimating driving performance based on EEG spectrum analysis, EURASIP J. Adv. Signal Process. 19 (2005) 3165–3174.

[10] N. Bobko, A. Karpenko, A. Gerasimov, V. Chernyuk, The mental performance of shiftworkers in nuclear and heat power plants of Ukraine, Int. J. Ind. Ergon. 12 (1998) 333–340.

[11] Y. Jou, T. Yenn, C.J. Lin, C. Yang, C. Chiang, Evaluation of operators' mental workload of human-system interface automation in the advanced nuclear power plants, Nucl. Eng. Des. 239 (2009) 2537–2542.

[12] J. Cannon, P.A. Krokhmal, Y. Chen, R. Murphey, Detection of temporal changes in psychophysiological data using statistical process control methods, Comput. Methods Prog. Biomed. 107 (2012) 367–381.

[13] F.T. Eggemeier, G.F. Wilson, Workload assessment in multi-task environments, in: D.L. Damos (Ed.), Multiple Task Performance, Taylor & Francis, London, 1991, pp. 207–216.

[14] A.F. Kramer, E.J. Sirevaag, R. Braune, A psychophysiological assessment of operator workload during simulated flight missions, Hum. Fact. 29 (1987) 145–160.

[15] C.D. Wickens, Engineering Psychology and Human Performance, HarperCollins Publishers, New York, 1992.

[16] H. Ayaz, P.A. Shewokis, S. Bunce, K. Izzetoglu, B. Willems, B. Onaral, Optical brain monitoring for operator training and mental workload assessment, NeuroImage 59 (2012) 36–47.

[17] A.T. Pope, E.H. Bogart, D.S. Bartolome, Biocybernetic system evaluates indices of operator engagement in automated task, Biol. Psychol. 40 (1995) 187–195.

[18] F.G. Freeman, P.J. Mikulka, L.J. Prinzel, M.W. Scerbo, Evaluation of an adaptive automation system using three EEG indices with a visual tracking task, Biol. Psychol. 50 (1999) 61–76.

[19] A. Haarmann, W. Boucsein, F. Schaefer, Combining electrodermal responses and cardiovascular measures for probing adaptive automation during simulated flight, Appl. Ergon. 40 (2009) 1026–1040.

[20] C.H. Ting, M. Mahfouf, A. Nassef, D.A. Linkens, G. Panoutsos, P. Nickel, A.C. Roberts, G.R.J. Hockey, Real-time adaptive automation system based on identification of operator functional state in simulated process control operations, IEEE Trans. Syst. Man Cyber. A Syst. Hum. 40 (2010) 251–262.

[21] A. Úbeda, E. Iáñez, J.M. Azorín, C. Perez-Vidal, Endogenous brain–machine interface based on the correlation of EEG maps, Comput. Methods Prog. Biomed. 112 (2013) 302–308.

[22] B. Hosseinifard, M.H. Moradi, R. Rostami, Classifying depression patients and normal subjects using machine learning techniques and nonlinear features from EEG signal, Comput. Methods Prog. Biomed. 109 (2013) 339–345.

[23] A. Brignol, T. Al-ani, X. Drouot, Phase space and power spectral approaches for EEG-based automatic sleep-wake classification in humans: a comparative study using short and standard epoch lengths, Comput. Methods Prog. Biomed. 109 (2013) 227–238.

[24] A. Kramer, Physiological metrics of mental workload: a review of recent progress, in: D.L. Damos (Ed.), Multiple Task Performance, Taylor & Francis, London, UK, 1991, pp. 279–328.

[25] N. Sharma, T. Gedeon, Objective measures, sensors and computational techniques for stress recognition and classification: a survey, Comput. Methods Prog. Biomed. 108 (2012) 1287–1301.

[26] S. Chen, J. Epps, Automatic classification of eye activity for cognitive load measurement with emotion interference, Comput. Methods Prog. Biomed. 110 (2013) 111–124.

[27] A. Gundel, G.F. Wilson, Topographical changes in the ongoing EEG related to the difficulty of mental tasks, Brain Topogr. 5 (1992) 17–25.

[28] M.K. Kiymik, M. Akin, A. Subasi, Automatic recognition of alertness level by using wavelet transform and artificial neural network, J. Neurosci. Methods 139 (2004) 231–240.

[29] A. Subasi, Automatic recognition of alertness level from EEG by using neural network and wavelet coefficients, Exp. Syst. Appl. 28 (2005) 701–711.

[30] E.A. Schmidt, M. Schrauf, M. Simona, M. Fritzsche, A. Buchner, W.E. Kincses, Drivers' misjudgement of vigilance state during prolonged monotonous daytime driving, Acc. Anal. Prevent. 41 (2009) 1087–1093.

[31] J.B. Noel, K.W. Bauer, J.W. Lanning, Improving pilot mental workload classification through feature exploitation and combination: a feasibility study, Comput. Oper. Res. 32 (2005) 2713–2730.

[32] J. Zhang, X. Wang, M. Mahfouf, D.A. Linkens, Fuzzy logic based identification of operator functional states using multiple physiological and performance measures, in: Proceedings of the International Conference on Biomedical Engineering and Informatics, Hainan, China, 2008, pp. 570–574.

[33] J.C. Christensen, J.R. Estepp, G.F. Wilson, C.A. Russell, The effects of day-to-day variability of physiological data on operator functional state classification, NeuroImage 59 (2012) 57–63.

[34] Y. Tomita, Y. Mitsukura, Hemodynamic characteristics for improvement of EEG-BCI performance, The 6th International IEEE Conference on Human System Interaction, June, 2013, pp. 495–500.

[35] B. Huang, A.H. Lo, B.E. Shi, Integrating EEG information improves performance of gaze based cursor control, The 6th International IEEE/EMBS Conference on Neural Engineering, November, 2013, pp. 415–418.

[36] G. Durantin, J.F. Gagnon, S. Tremblay, F. Dehais, Using near infrared spectroscopy and heart rate variability to detect mental overload, Behav. Brain Res. 259 (2014) 16–23.

[37] G.F. Wilson, F. Fisher, Cognitive task classification based upon topographic EEG data, Biol. Psychol. 40 (1995) 239–250.

[38] C.A. Russell, G.F. Wilson, Applications of Artificial Neural Networks for Air Traffic Controller Functional State

Classification, United States Air Force Research Laboratory, Dayton, USA, 2001, pp. 1–54.
[39] G.F. Wilson, C.A. Russell, Real-time assessment of mental workload using psychophysiological measures and artificial neural networks, Hum. Fact. 45 (2003) 635–644.
[40] M.V.M. Yeo, X. Li, K. Shen, E.P.V. Wilder-Smith, Can SVM be used for automatic EEG detection of drowsiness during car driving, Saf. Sci. 47 (2009) 115–124.
[41] G. Shou, L. Ding, D. Dasari, Probing neural activations from continuous EEG in a real-world task: time-frequency independent component analysis, J. Neurosci. Methods 209 (2012) 22–34.
[42] Z. Yin, J. Zhang, Operator functional state classification using least-square support vector machine based recursive feature elimination technique, Comput. Methods Prog. Biomed. 113 (2014) 101–115.
[43] R. Wang, J. Zhang, Y. Zhang, X. Wang, Assessment of human operator functional state using a novel differential evolution optimization based adaptive fuzzy model, Biomed. Sig. Process. Control 7 (2012) 490–498.
[44] R. Bellman, Adaptive Control Processes: A Guided Tour, Princeton University Press, Princeton, NJ, 1961.
[45] F. Camastra, Data dimensionality estimation methods: a survey, Pattern Recogn. 36 (2003) 2945–2954.
[46] G.V. Trunk, A problem of dimensionality: a simple example, IEEE Trans. Pattern Anal. Mach. Intell. 3 (1979) 306–307.
[47] S. Yang, J. Zhang, An adaptive human–machine control system based on multiple fuzzy predictive models of operator functional state, Biomed. Sig. Process. Control 8 (2013) 302–310.
[48] S.T. Roweis, L.K. Saul, Nonlinear dimensionality reduction by locally linear embedding, Science 290 (2000) 2323–2326.
[49] A. Ben-Hur, D. Horn, H.T. Siegelmann, V. Vapnik, Support vector clustering, J. Mach. Learn. Res. 2 (2001) 125–137.
[50] D.M.J. Tax, R.P.W. Duin, Support vector data description, Mach. Learn. 54 (2004) 45–66.
[51] B.Y. Sun, X.M. Zhang, J. Li, X.M. Mao, Feature fusion using locally linear embedding for classification, IEEE Trans. Neural Netw. 21 (2010) 163–168.
[52] D.D. Ridder, R.P.W. Duin, Locally Linear Embedding for Classification, Technical Report PH-2002-01, Delft University of Technology, 2002.
[53] H. Chang, D.Y. Yeung, Robust locally linear embedding, Pattern Recogn. 39 (2006) 1053–1065.
[54] J. Sauer, D.G. Wastell, G.R.J. Hockey, A conceptual framework for designing micro-worlds for complex work domains: a case study on the cabin air management system, Comput. Hum. Behav. 16 (2000) 45–58.
[55] B. Lorenz, F. Nocera, S. Röttger, R. Parasuraman, Automated fault-management in a simulated spacefight micro-world, Aviation Space Environ. Med. 73 (2002) 886–897.
[56] H.H. Jasper, Report of the committee on methods of clinical examination in electroencephalography, Electroencephalogr. Clin. Neurophysiol. 10 (1958) 370–375.
[57] D.G. Girton, J. Kamiya, A simple on-line technique for removing eye movement artifacts from the EEG, Electroencephalogr. Clin. Neurophysiol. 34 (1973) 212–216.
[58] O. Kouropteva, O. Okun, M. PietikSinen, Selection of the optimal parameter value for the locally linear embedding algorithm, in: Proceedings of 1st Internatational Conference on Fuzzy Systems and Knowledge Discovery, 2002, pp. 359–363.
[59] Z. Yin, J. Zhang, Identifying changes in human operator mental workload by locally linear embedding and support vector clustering approaches, in: Proceedings of 13th IFAC Symposium on Large Scale Complex Systems: Theory and Applications, Shanghai, China, 2013, pp. 353–358.
[60] J.A.K. Suykens, J. Brabanter, L. Lukas, J. Vandewalle, Weighted least squares support vector machines: robustness and sparse approximation, Neurocomputing 48 (2002) 85–105.
[61] Y. Pan, S.S. Ge, A.A. Mamun, F.R. Tang, Detection of seizures in EEG Signal using weighted locally linear embedding and SVM classifier, IEEE Conference on Cybernetics and Intelligent Systems, September, 2008, pp. 358–363.
[62] B.A. Lopour, S. Tasoglu, H.E. Kirsch, J.W. Sleigh, A.J. Szeri, A continuous mapping of sleep states through association of EEG with a mesoscale cortical model, J. Comput. Neurosci. 30 (2011) 471–487.
[63] F. Lee, R. Scherer, R. Leeb, A. Schlögl, H. Bischof, G. Pfurtscheller, Feature mapping using PCA, locally linear embedding and isometric feature mapping for EEG-based brain computer interface, in: Digital Imaging in Media and Education, Proceedings of the 28th AAPR Workshop, 2004.
[64] J.R. Mansfield, M.G. Sowa, G.B. Scarth, R.L. Somorjai, H.H. Mantsch, Fuzzy C-means clustering and principal component analysis of time series from near-infrared imaging of forearm ischemia, Comput. Med. Imaging Graph. 21 (1997) 299–308.
[65] J. Lee, C. Yoo, I. Lee, Statistical process monitoring with independent component analysis, J. Process Control 14 (2004) 467–485.
[66] C. Cajochen, D.P. Brunner, K. Kräuchi, P. Graw, A. Wirz-Justice, Power density in theta/alpha frequencies of the waking EEG progressively increases during sustained wakefulness, Sleep 18 (1995) 890–894.
[67] B.T. Jap, S. Lal, P. Fischer, E. Bekiaris, Using EEG spectral components to assess algorithms for detecting fatigue, Exp. Syst. Appl. 36 (2009) 2352–2359.
[68] J.A. Lee, M. Verleysen, Nonlinear Dimensionality Reduction, Springer, 2007.
[69] L. van der Maaten, E. Postma, J. van den Herik, Dimensionality Reduction: A Comparative Review, Technical Report 2009-005, Tilburg University, 2009.
[70] B. Mulder, A. Kruizinga, S. Arjan, I. Vernema, P. Hoogeboom, Monitoring cardiovascular state changes in a simulated ambulance dispatch task for use in adaptive automation, in: D. de Waard, K.A. Brookhuis, C.M. Weikert (Eds.), Human Factors in Design, Shaker, Maastricht, the Netherlands, 2004, pp. 161–175.
[71] L.J.M. Mulder, C. Dijksterhuis, A. Stuiver, D. de Waard, Cardiovascular state changes during performance of a simulated ambulance dispatchers' task: potential use for adaptive support, Appl. Ergon. 40 (2009) 965–977.
[72] A. Hoover, A. Singh, S. Fishel-Brown, E. Muth, Real-time detection of workload changes using heart rate variability, Biomed. Signal Process. Control 7 (2012) 333–341.